

A High-Throughput AES-GCM Implementation on GPUs for Secure, Policy-Based Access to Massive Astronomical Catalogs

Samuel Lemes-Perera^{a,b,c,*}, Miguel R. Alarcon^{a,d,e}, Pino Caballero-Gil^b, Miquel Serra-Ricart^{a,d,e}

^aLight Bridges S.L., Observatorio Astronómico del Teide, Carretera del Observatorio del Teide, s/n, Santa Cruz de Tenerife, E-38500, Spain

^bDepartamento de Ingeniería Informática y de Sistemas, Universidad de La Laguna (ULL), Calle Padre Herrera s/n, San Cristóbal de La Laguna, E-38206, Spain

^cInstituto Tecnológico y de Energías Renovables (ITER), Polígono Industrial de Granadilla s/n, Granadilla de Abona, E-38600, Spain

^dInstituto de Astrofísica de Canarias (IAC), C/Vía Láctea s/n, San Cristóbal de La Laguna, E-38205, Spain

^eDepartamento de Astrofísica, Universidad de La Laguna (ULL), Av. Astrofísico Francisco Sánchez s/n, San Cristóbal de La Laguna, E-38206, Spain

Abstract

The era of large astronomical surveys generates massive image catalogs requiring efficient and secure access, particularly during pre-publication periods where data confidentiality and integrity are paramount. While Findable, Accessible, Interoperable, and Reusable (FAIR) principles guide the eventual public dissemination of data, traditional security methods for restricted phases often lack granularity or incur prohibitive performance penalties. To address this, we present a framework that integrates a flexible policy engine for fine-grained access control with a novel GPU-accelerated implementation of the AES-GCM authenticated encryption protocol.

The novelty of this work lies in the adaptation and optimization of a parallel tree-reduction strategy to overcome the main performance bottleneck in authenticated encryption on GPUs: the inherently sequential Galois/Counter Mode (GCM) authentication hash (GHASH). We present both the algorithmic adaptation and its efficient execution on GPU architectures. Although similar parallelization techniques have been explored in cryptographic research, this is, to our knowledge, the first demonstration of their integration into a high-throughput encryption framework specifically designed for large-scale astronomical data. Our implementation transforms the sequential GHASH computation into a highly parallelizable, logarithmic-time process, achieving authenticated encryption throughput suitable for petabyte-scale image analysis.

Our solution provides a robust mechanism for data providers to enforce access policies, ensuring both confidentiality and integrity without hindering research workflows, thereby facilitating a secure and managed transition of data to public, FAIR archives.

Keywords:

Astronomical Catalogs, Data Security, GPU Acceleration, Cryptography, AES-GCM, Policy Enforcement, FITS

1. Introduction

Modern astronomy, driven by large-scale surveys such as the Legacy Survey of Space and Time (LSST), is generating petabyte-scale image catalogs (Ivezić et al., 2019; Berriman and Groom, 2011). While these massive datasets are the engine of discovery, they introduce critical challenges in data security and access control, particularly during the embargo and validation phases that necessarily precede public release. Protecting sensitive data during proprietary periods, enforcing granular collaboration policies, and ensuring the priority of discoveries are paramount requirements before data fully adheres to the Findable, Accessible, Interoperable, and Reusable (FAIR) principles in public archives (Wilkinson et al., 2016; Chen et al., 2022).

The risks associated with inadequate data protection are vividly illustrated by historical incidents ranging from ethical breaches to infrastructure attacks. The controversy surrounding the discovery of the dwarf planet Haumea (Brown et al.,

2005, 2007) highlighted how unauthorized access to observation logs can lead to priority disputes, undermining scientific integrity. More recently, the vulnerability of astronomical infrastructure was underscored by the 2022 cyberattack on the Atacama Large Millimeter/submillimeter Array (ALMA), which forced a suspension of scientific operations and data delivery, demonstrating that major facilities are targets for direct cyber threats (National Radio Astronomy Observatory, 2022). Similarly, the risks of utilizing unvalidated, preliminary data products were highlighted by the BICEP2/Planck controversy (Ade and et al., 2014, 2015).

Beyond preventing malicious incidents, robust access control is a standard operational requirement for major facilities. Missions and observatories such as the James Webb Space Telescope, Euclid, ALMA, and LSST enforce specific data rights policies that include proprietary periods ranging from months to years. During these phases, data access must be strictly limited to Principal Investigators or consortium members for calibration and initial scientific exploitation. Furthermore, modern large-scale collaborations require granular permission management, distinguishing between core team members, external col-

*Corresponding author

Email address: samuel@lightbridges.es (Samuel Lemes-Perera)

laborators, and students, while simultaneously guaranteeing the integrity and authenticity of the data against corruption or tampering.

However, the imperative to secure these datasets often conflicts with the high-throughput access demanded by modern scientific workflows. Traditional cryptographic measures can impose significant computational overhead (latency and reduced bandwidth), creating unacceptable bottlenecks for data-intensive analysis. Addressing this dual challenge requires solutions that provide robust, fine-grained access control without compromising the I/O performance required by High-Performance Computing (HPC) environments.

To address this, we present a framework that integrates a flexible policy engine for access control with a novel, high-throughput GPU-accelerated implementation of the AES-GCM (Galois/Counter Mode) protocol (Dworkin, 2007; Salowey et al., 2008). Securing high-resolution astronomical images presents unique challenges: the sheer volume of pixel data requires algorithms that can sustain multi-gigabit throughput to avoid I/O starvation, while the structured nature of FITS files demands mechanisms to prevent pattern leakage. AES-GCM is widely recommended for such high-bandwidth applications because it combines the parallelizability of Counter Mode, essential for handling large payloads efficiently, with a built-in integrity check that detects data corruption without the overhead of a separate HMAC pass (McGrew and Viega, 2004; An and Seo, 2020). Unlike simpler modes, such as Counter (CTR) that provide only *confidentiality*, AES-GCM provides Authenticated Encryption with Associated Data (AEAD), ensuring both confidentiality and data integrity.

The primary technical challenge of this approach, and the core contribution of our work, is overcoming the performance bottleneck inherent in AES-GCM’s authentication component: the GHASH function. GHASH operates by chaining multiplications over a binary Galois Field ($GF(2^{128})$) to compute a message authentication code. While mathematically robust, this chain implies that the processing of each data block strictly depends on the result of the previous one. Consequently, the standard GHASH algorithm is inherently sequential, making it ill-suited for the massive parallelism of Graphics Processing Units (GPUs) (Manavski, 2007; Lee et al., 2025). Following the strategy described by Lee et al. (2025), we transform the linear $O(N)$ GHASH computation into a scalable, logarithmic-time $O(\log N)$ process. This enables authenticated encryption at throughputs matching the I/O capabilities of modern storage systems.

Our framework assumes the existence of a secure, external Key Management Service (KMS) for key provisioning, focusing strictly on the cryptographic performance and policy enforcement layer. This solution offers a robust mechanism for data providers to enforce access policies during sensitive periods, ensuring both confidentiality and integrity without hindering research workflows, thereby facilitating a secure and managed transition of data to public, FAIR archives.

The remainder of this paper describes the data context and access challenges (Section 2), details the framework’s architecture (Section 3), its mechanisms for secure access (Section 4),

the specifics of our GPU-accelerated implementation and its performance benchmarks (Section 5), followed by a discussion (Section 6) and some conclusions (Section 7).

2. Data Context and Access Challenges

The framework operates within the specific context of modern astronomical data archives, particularly those dominated by large image catalogs. Understanding the nature of this data and the typical ways astronomers interact with it is crucial for appreciating the security and performance challenges involved.

2.1. Characteristics of Astronomical Image Catalogs

The vast majority of astronomical image data, from ground-based telescopes to space missions, adheres to the Flexible Image Transport System (FITS) standard (Greisen et al., 1980; Wells et al., 1981; Ponz et al., 1994; IAU FITS Working Group, 2016). FITS provides a crucial structure based on Header/Data Units (HDUs), recognizing the distinct yet complementary roles of metadata and pixel arrays in scientific analysis. Typically, a FITS file contains a primary HDU holding the main image array (the core scientific data, e.g., pixel values) and its associated descriptive header. Additional extensions can follow, containing other data arrays (like weight maps or masks) or binary tables, each with their own header.

Critically, the header sections store essential metadata as keyword/value pairs. This includes observational parameters (telescope telemetry, instrument configuration, exposure time, filters), processing history (calibration steps, software versions), and arguably most importantly, the World Coordinate System (WCS) information (Greisen and Calabretta, 2002; Calabretta and Greisen, 2002) and flux calibration (Analog-to-Digital Units, ADU, to magnitudes). The WCS maps pixel coordinates to celestial coordinates (e.g., Right Ascension and Declination), while flux calibration enables the conversion of pixel values to physical units. This rich metadata is often as scientifically valuable as the pixel data itself, enabling data discovery and context, thus necessitating careful consideration in any security framework regarding how both components are accessed and protected.

The scale of data generation in modern astronomy is expanding rapidly across all tiers of observation. This trend is evident in agile, high-cadence robotic facilities such as the Two-meter Twin Telescope (TTT)¹ and the Transient Survey Telescope (TST)², as well as in massive synoptic surveys like LSST (Ivezić et al., 2019), Pan-STARRS (Chambers et al., 2016), ZTF (Bellm et al., 2019; Yao et al., 2019), and space missions like Euclid (Laureijs et al., 2011). Collectively, these projects generate enormous quantities of FITS data, where individual images can range from megabytes to gigabytes. Archives routinely host millions of such files, pushing total data volumes into the petabyte and exabyte scales (Berriman and Groom, 2011). Managing, querying, and accessing this data efficiently

¹<https://ttt.iac.es>

²<https://tst.iac.es>

is a significant challenge that is further complicated when strict security requirements are applied.

2.2. Common Data Access Patterns and Security Integration

Astronomers interact with image archives in various ways, each presenting different implications for integrating security measures:

- **Full File Retrieval:** Users often download entire FITS files for local processing. For security, this implies decrypting the complete file, requiring efficient throughput handling for potentially large files (e.g., >500MB).
- **Metadata Queries:** Researchers frequently search and retrieve information solely from FITS headers (e.g., finding all observations of a specific object or within a certain time range) without immediately needing the pixel data. Security policies might allow broader access to metadata while restricting pixel data access. The framework must therefore be able to differentiate between HDU types, allowing performant decryption of headers without the overhead of decrypting the full data payload.
- **Direct/Streaming Analysis:** Modern workflows increasingly utilize libraries (e.g., Astropy (Collaboration, 2013, 2018)) or server-side platforms to access and analyze data arrays directly, potentially without creating intermediate files on disk. The security layer must integrate transparently with these tools, performing decryption on-the-fly as data is read or streamed into memory.

A successful security framework must accommodate these diverse patterns, providing protection without unduly hindering common scientific workflows or introducing prohibitive performance penalties, especially for interactive analysis or large-scale processing pipelines.

2.3. Limitations of Existing Security Approaches and the Role of FAIR Principles

Current security practices in many astronomical archives often fall short of providing the required granularity, performance, and transparency for data during restricted phases:

- **Perimeter Security (VPNs, Firewalls):** While useful for network-level protection, these offer coarse-grained ("all-or-nothing") access once a user is authenticated within the perimeter. They do not provide fine-grained control over specific datasets or enforce complex policies, nor do they protect data once it has been downloaded or moved.
- **Web Portal Authentication:** Basic username/password access to data portals often lacks granular authorization based on data properties or user roles beyond the initial login. Furthermore, data downloaded through such portals is typically unprotected thereafter ("data at rest").

- **Operating System Filesystem Permissions:** Standard Portable Operating System Interface permissions are insufficiently expressive to capture complex scientific access policies (e.g., time-based embargoes, role-based access tied to collaboration status). Managing these permissions across petabyte-scale archives with millions of files is administratively unscalable.
- **Lack of Widespread Encryption:** Due to perceived performance overheads and the complexity of key management, end-to-end encryption of large scientific data archives is not yet common practice. Data is often stored unencrypted, leaving it vulnerable if storage systems are compromised or physical media is lost.
- **Alignment with Open Science Goals:** While the community strongly moves towards Open Science and FAIR data principles (Wilkinson et al., 2016; Chen et al., 2022), facilitated by public archives (Green et al., 2024), these principles primarily apply once data enters the public domain. Existing mechanisms often lack dedicated solutions to robustly manage the *transition phases*, embargo periods, collaborative analysis, pre-publication review, where controlled, secure access is temporarily necessary before full public release.

These limitations highlight the need for a dedicated framework that bridges the gap, integrating strong, policy-driven access control directly with performant cryptographic protection at the data level. This ensures security during the research phase while facilitating a smooth eventual transition towards public, FAIR accessibility.

3. Framework Architecture

To address the dual challenges of security and performance in astronomical archives, a modular framework designed for seamless integration with existing data centers is proposed. The architecture strictly separates the concerns of policy enforcement (Control Plane) from high-performance cryptographic execution (Data Plane). Figure 1 illustrates the complete system architecture, detailing the interaction flow between the conceptual components and the parallel cryptographic streams. While this paper focuses on the implementation and performance of the GPU-accelerated cryptographic library, the architectural context is essential to understand how granular access is enforced.

The data access workflow follows a strict "verify-then-decrypt" orchestration. An application's request is intercepted by an Access Control Module (ACM), which validates the user's identity and queries a Policy Engine. Upon a GRANT decision, the ACM retrieves the specific decryption keys from an external KMS and passes them to the Cryptographic Module. This module then executes the high-throughput, GPU-accelerated decryption and integrity verification, returning the plaintext FITS data to the application only if both the identity authorization and the cryptographic signature verification succeed.

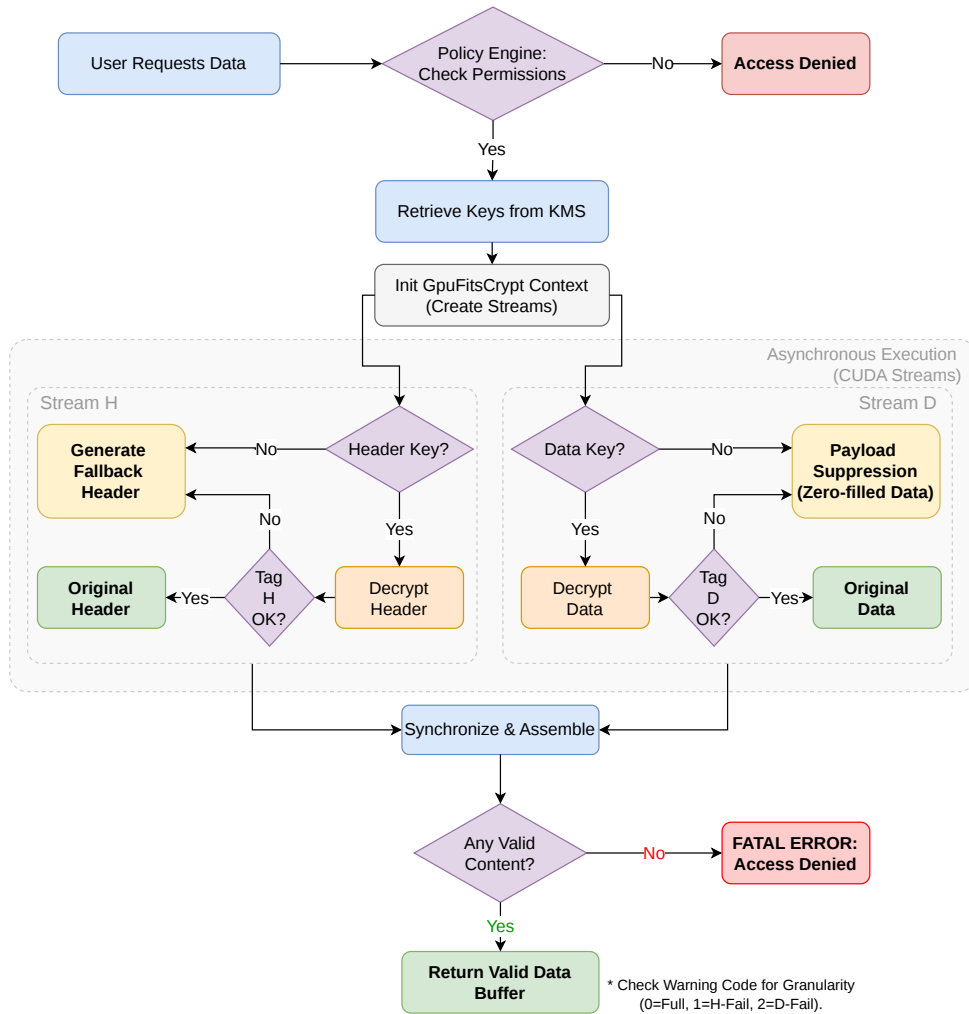


Figure 1: Architecture and granular enforcement workflow. The diagram integrates the Control Plane components with the parallel Data Plane execution. Unlike monolithic approaches, it illustrates the compartmentalized verification logic: specific keys determine the execution path in independent streams (H/D). Crucially, the workflow demonstrates the fail-safe mechanisms: absence of a Data Key or integrity failure triggers Payload Suppression (zero-filling), while Header issues activate Fallback Header generation, ensuring a valid FITS container is returned even in partial access scenarios.

3.1. Conceptual Components: The Control Plane

The framework relies on three conceptual components to manage authorization and key distribution, ensuring that cryptographic operations are policy-driven rather than ad-hoc.

- **Policy Engine:** This module acts as the authorization brain, storing and evaluating granular access rules. Policies link user identities (e.g., Co-Investigators, Students) to data attributes (e.g., `release_date`, `proposal_id`) using logic such as `allow access if (user.role == 'collaborator' AND data.embargo_active == true)`. It returns a binary GRANT or DENY decision.
- **Access Control Module:** The ACM serves as the Application Programming Interface (API) gateway and orchestrator. It handles authentication, requests policy decisions, and interfaces with the KMS. Crucially, it isolates the keys

from the end-user; the user never sees the raw key, only the resulting data stream.

- **Key Management Service Interface:** The architecture assumes the existence of a secure, industry-standard KMS (e.g., HashiCorp Vault, AWS KMS). The framework abstracts key generation and lifecycle management, interacting with the KMS strictly to retrieve keys for authorized sessions.

3.2. The Cryptographic Module: *GpuFitsCrypt*

The core technical contribution of this work is the implementation of the data plane: a high-performance C++/CUDA library named *GpuFitsCrypt*. This library handles the computationally intensive tasks of encryption, decryption, and authentication.

3.2.1. Cryptographic Protocol: AES-GCM

The framework implements the AES-128-GCM standard (Dworkin, 2007). Unlike the CTR mode used in early prototypes which provided only confidentiality, GCM is an AEAD mode. It generates a 128-bit Authentication Tag that guarantees both the confidentiality of the pixel data and the integrity of the file. This ensures that any unauthorized modification to the encrypted payload or the metadata is immediately detected (resulting in a decryption failure), a critical requirement for scientific data provenance and validation.

3.2.2. Authenticated FITS File Format

To support granular access while maintaining the integrity of the file structure, a custom FITS encapsulation format is employed (see Figure 2). The original FITS file is transformed into a two-HDU structure:

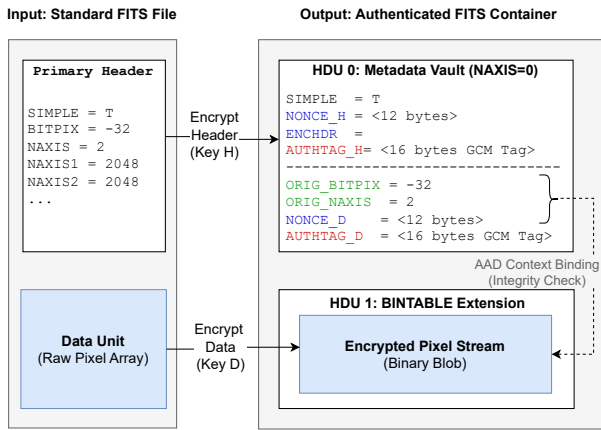


Figure 2: **Structure of the Authenticated FITS Format.** The original file (left) is split into a dual-key container (right). The Primary HDU (HDU 0) acts as a metadata vault, storing cryptographic nonces, authentication tags, and the original header encrypted within the ENCHDR keyword. Critical structural metadata (ORIG_*) remains in plaintext to allow file parsing but is cryptographically bound to the encrypted pixel data (HDU 1) via the AES-GCM Associated Data (AAD) mechanism. This ensures that any tampering with the plaintext WCS or dimensions triggers an authentication failure in AUTHTAG_D.

1. Primary HDU (Metadata Container): A metadata-only HDU (NAXIS=0) acting as a secure envelope containing:

- NONCE_H and NONCE_D: 96-bit (12-byte) initialization vectors generated via a Cryptographically Secure Pseudo-Random Number Generator. These ensure uniqueness for the header and data encryption operations, respectively.
- ENCHDR: The complete original FITS header, encrypted with the Header Key.
- AUTHTAG_H: The 128-bit GCM authentication tag verifying the integrity of ENCHDR.
- ORIG_*: Plaintext copies of essential structural keywords (e.g., ORIG_NAXIS, ORIG_BITPIX) required to parse the file structure before decryption.

- AUTHTAG_D: The 128-bit GCM authentication tag protecting the encrypted pixel data and its associated metadata context.

2. BINTABLE Extension (Data Container): The original pixel array is encrypted with the Data Key and stored as a Binary Large Object (BLOB) in a single-row Binary Table extension.

Nonce Generation and Uniqueness Assurance: The security of the AES-GCM mode relies strictly on the uniqueness of the initialization vector for a given key. To eliminate the risk of nonce reuse, the framework employs a stochastic generation approach compliant with NIST SP 800-38D guidelines (Dworkin, 2007). The 96-bit nonces are generated utilizing the host system’s entropy pool (e.g., via /dev/urandom). Given the 96-bit namespace, the probability of a collision remains negligible ($< 10^{-12}$) even for archives scaling to billions of files, thereby ensuring operational security without requiring centralized state management for nonce counters.

This dual-key design allows a Policy Engine to grant access to the header (e.g., for query validation) without releasing the key for the scientific pixel data.

3.2.3. Context Binding via Associated Data (AAD)

A unique feature of the implementation is the use of GCM’s Associated Data (AAD) capability to cryptographically bind the plaintext metadata to the encrypted pixels. The library constructs the AAD vector for the data payload by concatenating the data Nonce with the string representation of the critical structural keywords:

$$\text{AAD}_{\text{Data}} = \text{NONCE}_D \parallel \text{Serialize}(\text{ORIG_BITPIX}) \parallel \text{Serialize}(\text{ORIG_NAXIS}) \parallel \dots$$

where the $\text{Serialize}(\cdot)$ function converts numerical values to their strict ASCII decimal representation (e.g., the integer -32 becomes the byte sequence $'-32'$), eliminating potential ambiguities arising from padding spaces or formatting variances.

This AAD is fed into the GHASH computation during both encryption and decryption. While the ORIG_* keywords remain readable in the header to allow standard FITS tools to identify the file size, any tampering with these values (e.g., altering the coordinate system or exposure time) causes the computed hash to diverge from AUTHTAG_D. This prevents “context swapping attacks,” ensuring the scientific data cannot be presented with falsified telemetry.

Application Programming Interface. The library exposes a C-style API designed for integration with high-level languages like Python. As shown in Table 1, the interface abstracts the complexity of GPU memory management and GCM tag verification.

3.3. GPU Acceleration Strategy

Achieving high throughput with AES-GCM on large files requires masking the latency of memory transfers and overcoming the inherently serial nature of the authentication phase.

Table 1: Core functions and data structures of the `GpuFitsCrypt` library. The API is designed to return granular status codes, enabling applications to distinguish between full access, partial access (metadata only), and security failures.

Component	Description
<i>Functions</i>	
<code>gfc_context_create</code>	Initializes session: pre-allocates pinned memory and CUDA streams.
<code>gfc_decrypt_frame</code>	Decrypts and authenticates a FITS frame. Returns <code>FitsOperationResult</code> .
<code>gfc_context_destroy</code>	Teardown: releases all GPU and host resources.
<i>Data Structures: <code>FitsOperationResult</code></i>	
<code>data_buffer</code>	Pointer to the decrypted FITS file in memory (ready for Astropy).
<code>error_code</code>	0: Success (check warning); <0: System/IO Error.
<code>warning_code</code>	0: Full Access; 1: Header Fallback; 2: Payload Suppressed (Data Key mismatch).

3.3.1. Parallel GHASH Reduction

The standard GHASH algorithm operates via a serial chain defined by the recurrence relation:

$$Y_i = (Y_{i-1} \oplus X_i) \cdot H \quad (1)$$

where Y_i is the 128-bit authentication tag accumulator at step i , Y_{i-1} is the previous state, X_i represents the current 128-bit input block (which can be either Associated Data or Ciphertext), \oplus denotes the bitwise XOR operation, and \cdot represents multiplication in the Galois Field $GF(2^{128})$ using the precomputed hash subkey H .

This serial dependency implies that the processing of block i cannot strictly begin until block $i - 1$ is complete (see Figure 3-a), making it typically ill-suited for the massive parallelism of GPUs. To address this, the implementation utilizes a parallel reduction strategy operating in the Galois Field $GF(2^{128})$, inspired by recent optimizations for parallel architectures (Lee et al., 2025).

The library precomputes a table of powers of the hash key H ($H^{2^0}, H^{2^1}, H^{2^2}, \dots, H^{2^k}$). This sequence corresponds to the stride length at each level of a binary reduction tree. As illustrated in Figure 3-b, this enables the input data to be split into independent blocks and combined in a hierarchical manner. Instead of a linear dependency chain, GPU threads compute partial hashes concurrently, multiplying by the appropriate power of H to "jump" gaps in the sequence. This reduces the computational complexity from linear time $O(N)$ to logarithmic time $O(\log N)$, effectively matching the throughput of the counter-mode encryption component.

3.3.2. Asynchronous Streams Pipeline

The library implements an asynchronous pipeline using NVIDIA CUDA streams to overlap host-device communication with computation:

1. **Dual-Stream Context:** The library maintains a persistent context with two concurrent CUDA streams: `streamH` (Header) and `streamD` (Data), along with Pinned Memory (page-locked) host buffers to maximize PCIe bandwidth.
2. **Header Processing:** `streamH` handles the ENCHDR decryption. Since headers are typically small (< 80 kB), this provides low-latency access to metadata.
3. **Data Pipeline:** `streamD` manages the heavy lifting for the pixel data. The host reads the encrypted BLOB directly into pinned memory. The stream then executes the GCM pipeline:
 - **H-Power Generation:** Computes powers of the authentication key on the fly if the data size requires it.
 - **AES-CTR Kernel:** Generates the keystream and decrypts the payload in parallel blocks.
 - **GHASH Kernel:** Performs the parallel reduction on the ciphertext and AAD to verify integrity.
4. **Validation Gate:** The library enforces a strict validation gate. The output buffer is only marked as valid if the locally computed GHASH matches the AUTHTAG stored in the file. If verification fails, the operation returns a distinct integrity error code, ensuring no corrupted or manipulated data is released to the user.

4. Secure and Transparent Data Access

The primary goal of the framework is to provide robust security and granular access control without imposing a significant burden on the end-user. This is achieved through a combination of a transparency mechanism at the application layer and a strict policy enforcement workflow. This section describes the user interaction model and how the dual-key FITS format enables diverse and efficient access patterns.

4.1. User Interaction and Transparency Mechanism

From the perspective of a research scientist, interacting with the encrypted data archive must be seamless. The complexity of decryption, key handling, and policy checks is abstracted away by the framework's interface. The implementation provides a C-style API (refer to Table 1) designed to be wrapped by higher-level languages commonly used in astronomy, such as Python.

Listing 1 (Appendix A.1) demonstrates a typical user workflow. The user initializes a session context once at the beginning, pre-allocating necessary GPU and pinned memory resources via `gfc_context_create`. For each encrypted FITS file, the `gfc_decrypt_frame` function is called. Upon success, the library returns a `FitsOperationResult` structure containing a pointer to a fully decrypted FITS file in memory.

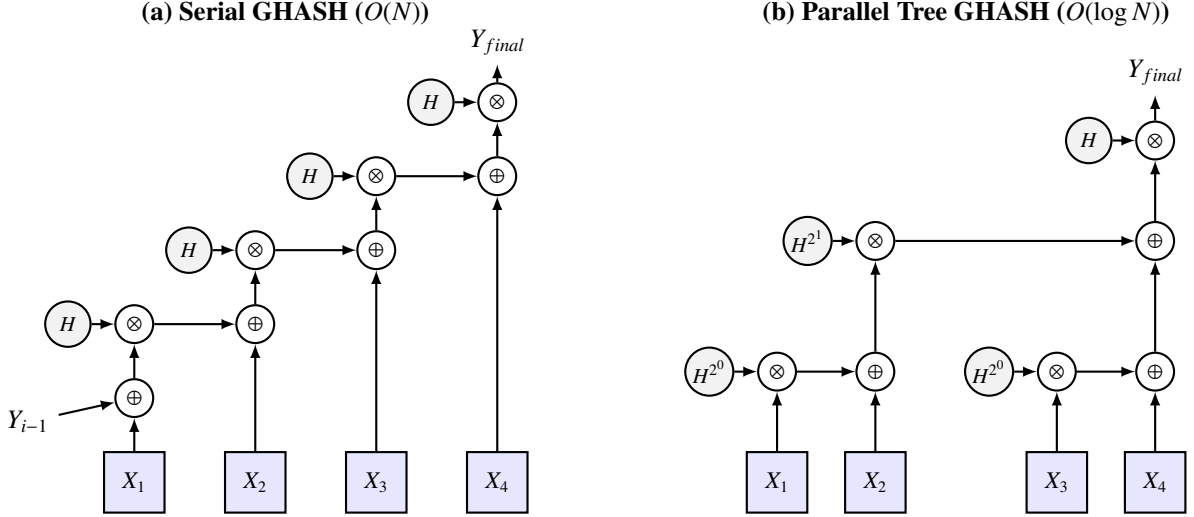


Figure 3: Comparison of GHASH strategies. (a) The standard serial approach creates a dependency chain where each step waits for the previous one. (b) The proposed parallel approach uses a binary reduction tree. By precomputing powers of H (H^{2^0}, H^{2^1}, \dots), independent blocks can be combined in parallel steps ($O(\log N)$), saturating the GPU cores.

This memory buffer can be passed directly to standard scientific libraries like `Astropy` using memory-efficient methods such as `HDUList.fromstring()`, treating the decrypted data as a virtual file. This approach achieves a high degree of transparency; the analysis code interacts with standard data objects, remaining agnostic to the underlying cryptographic operations.

4.2. Policy Enforcement and Granular Access

The framework’s ability to enforce fine-grained access control is predicated on the dual-key design of the encrypted FITS format, orchestrated by the architecture’s Control Plane. As depicted in the workflow diagram (Figure 1 in Section 3), abstract policy rules are translated into concrete cryptographic operations through a conditional key release mechanism.

Consider a scenario involving a dataset under a proprietary period. Table 2 illustrates how different user roles and policies translate into the specific keys provisioned by the Access Control Module (ACM) and the resulting data access level provided by the library.

A critical feature of the Policy Engine is its support for time-based rules, essential for automating data embargoes. As shown in Table 2, a “Public User” is initially denied access. However, a rule such as `allow role:public if data.release_date < now()` automatically transitions the access level upon the embargo’s expiration. After this date, the same request results in the provisioning of both keys, granting `FULL_ACCESS`.

Furthermore, the model allows decoupling metadata access from pixel data access. A collaborator may be granted the Header Key to decrypt the `ENCHDR` keyword, enabling analysis of observational telemetry without accessing the scientific pixel data. Conversely, to support blind analysis scenarios where metadata is restricted, the library implements an automatic fallback mechanism. If the Header Key is denied (or incorrect), the library constructs a structurally valid, minimal

FITS header in memory using the unencrypted `ORIG_*` keywords (e.g., `ORIG_NAXIS`, `ORIG_BITPIX`). This ensures that even with restricted permissions, the user receives a parsable FITS file, preserving compatibility with standard tools while keeping the core scientific content secure.

Crucially, unlike confidentiality-only modes such as `AES-CTR`, the use of `AES-GCM` ensures data integrity through compartmentalized verification. In our implementation, the integrity checks for metadata and pixel data are decoupled. Consequently, a mismatch in the Data Key (or integrity failure) triggers a payload suppression mechanism: the library returns a structurally valid FITS object where the scientific pixel array is zero-filled (physically suppressed via `memset`), while the authenticated header remains fully accessible.

This mechanism, combined with the automatic header fallback described above, ensures that granular access policies are enforced without crashing the read operation or exposing the application to corrupted content, maintaining compatibility with standard FITS viewers even in restricted access scenarios.

5. GPU-Accelerated Cryptography Implementation and Performance

This section details the technical implementation of the `GpuFitsCrypt` module and presents a comprehensive performance analysis. The discussion focuses on the specific strategies employed to parallelize the authenticated encryption process on the GPU and the resulting throughput across consumer and datacenter hardware tiers.

5.1. Choice of Cryptographic Mode

We selected `AES-128-GCM` (Galois/Counter Mode) as the cryptographic standard. While Counter (CTR) mode offers high parallelizability and confidentiality, it lacks intrinsic integrity verification, leaving scientific data vulnerable to ciphertext manipulation (e.g., bit-flipping attacks) unless paired with a

Table 2: Role-based and temporal access control policies. The table reflects the full granularity of the system, demonstrating how different key combinations trigger specific behaviors (Full Access, Suppression, or Fallback).

Scenario / Role	Policy Context	KMS Key Provisioning	Resulting Access / System Behavior
Principal Inv.	FULL_ACCESS	Header + Data Key	Full Access: Metadata and Pixels fully decrypted and authenticated.
Archive Miner	METADATA_ONLY	Header Key Only	Payload Suppression: Header authenticated; Pixel data physically zeroed to protect IP.
Blind Analysis	PIXELS_ONLY (Sensitive Telemetry)	Data Key Only	Header Fallback: Minimal header reconstructed from plaintext; Pixels decrypted.
Integrity Check	role:any on data:tampered	Header + Data Key	Auth Failure: GHASH mismatch triggers suppression. Safety mechanism active.

separate Message Authentication Code (MAC). GCM provides Authenticated Encryption with Associated Data, guaranteeing both confidentiality and integrity in a single, efficient pass. The primary challenge addressed in this work is the efficient parallelization of GCM’s authentication component, GHASH, which is inherently sequential.

5.2. GPU Implementation: Parallel GHASH Architecture

The `GpuFitsCrypt` library utilizes the NVIDIA CUDA platform. Building upon the high-performance bit-sliced AES-CTR core architecture described by Lee et al. (2024), we introduced a critical modification to ensure cryptographic interoperability across heterogeneous hardware. The original algorithm’s counter generation logic was coupled to the GPU grid geometry (total thread count), causing the keystream to vary with hardware configuration. We refactored the kernel to enforce a deterministic, geometry-agnostic mapping between data blocks and AES counters. This ensures that a FITS file encrypted on an edge device (e.g., Jetson Nano) can be correctly decrypted on a datacenter GPU (e.g., NVIDIA A100), regardless of the parallelism degree, without compromising the high-throughput performance. One of the core innovations of this work lies in transforming the serial GHASH dependency chain (Equation 1) into a parallelizable workload suitable for massive datasets.

5.2.1. Parallel Tree-Reduction Strategy

Inspired by recent optimizations for parallel architectures (Lee et al., 2025), we implement the reduction strategy operating in the Galois Field $GF(2^{128})$ as theoretically defined in Section 3.

- **Precomputation:** The library generates the look-up table of hash key powers (corresponding to the stride lengths H^{2^k} described in Section 3.3.1) on the GPU. This pre-calculated table allows any data block in the sequence to be processed independently, effectively bridging the positional gap without serial dependencies.

- **Tree Reduction Kernel:** Our custom kernel, `ghash_parallel_reduction`, leverages Shared Memory to load data chunks, minimizing global memory latency. It then performs the synchronized tree reduction (visualized in Figure 3-b). In each step, threads combine partial results using the precomputed powers, reducing the complexity from linear $O(N)$ to logarithmic $O(\log N)$.

5.2.2. Scalable MapReduce for Massive Files

Since a single CUDA block cannot process an arbitrary number of data blocks due to shared memory limits, we employ a two-phase MapReduce architecture to handle large FITS files (e.g., 600 MB to 3 GB):

1. **Map Phase (Partial Reduction):** A grid of CUDA blocks is launched. Each block processes a fixed segment of the input data (ciphertext + AAD) independently, producing a single 16-byte partial hash.
2. **Reduce Phase (Final Combination):** A secondary kernel, `combine_partial_ghash`, takes the array of partial hashes and combines them on the GPU. This architecture prevents the latency of transferring intermediate results back to the CPU, keeping the entire authentication pipeline on the device.

5.2.3. Optimized Memory Pipeline

To ensure the GPU is fed data at a rate matching its compute capability, the implementation utilizes:

- **Pinned Memory I/O:** All host buffers use page-locked memory (`cudaMallocHost`) to maximize PCIe bandwidth and enable Direct Memory Access.
- **Dual-Stream Overlap:** As detailed in Section 3, encryption/decryption (AES-CTR) and authentication (GHASH) are managed within a stream pipeline that overlaps with disk I/O operations.

5.3. Performance Benchmarking

We evaluated the framework on a diverse set of hardware, ranging from edge/mobile GPUs to datacenter accelerators (see Table A.5 in Appendix A.3 for hardware specs). The dataset consisted of both real and synthetic FITS images ranging from 16 MB to approximately 600 MB (Large) and 3.4 GB (Extra-Large) (see Table A.6).

5.3.1. Experimental Protocol

To ensure statistical robustness and reproducibility, a rigorous measurement protocol was applied to all reported benchmarks:

- **Execution Context:** The CUDA context, including pinned memory allocation and stream creation, was initialized once per session and reused across all runs. This ensures that measurements reflect the steady-state performance of the pipeline, excluding the one-time overhead of driver initialization and context creation.
- **Sampling Strategy:** For every hardware and file size configuration, we performed 5 warm-up runs (discarded) to stabilize GPU clock states and JIT compilation effects, followed by 200 timed repetitions. Reported values represent the median of these executions, accompanied by standard deviations to quantify variability.
- **Timing Mechanisms:** GPU kernel execution times were measured using high-precision `cudaEventRecord` pairs on the device stream. Host-side End-to-End latencies were recorded using monotonic system timers (e.g., `time.monotonic()` in Python) to capture the full wall-clock duration experienced by the user.

5.3.2. Performance Metrics Definition

To accurately characterize the system’s behavior across different bottlenecks, we define three distinct metrics used in the analysis:

1. **Kernel Time:** Represents the exclusive execution duration of the decryption and authentication kernels on the GPU. This metric isolates raw computational throughput from system I/O.
2. **End-to-End (E2E) Time:** Measures the total time from the initial API call until the decrypted data is fully available in system RAM. This includes disk I/O, host-to-device PCIe transfers, kernel execution, and Python runtime overhead.
3. **Net Cryptographic Cost:** Defined as $(E2E_{GCM} - \text{Astropy}_{Load})$. This metric isolates the computational overhead of the security layer by subtracting the baseline I/O cost of loading a standard unencrypted FITS file via `Astropy`. It serves as a proxy for the "price of security" in a production pipeline.

Table 3: Kernel-optimal parameters and execution time for AES-GCM on the large FITS dataset (≈ 600 MB). Note that for this workload size, the execution time on Datacenter GPUs (H100, A100) is dominated by kernel launch latency rather than computational throughput, resulting in times comparable to consumer cards.

GPU Model	Opt. TS	Opt. R	Kernel Time (s)
<i>Datacenter / HPC</i>			
H100 PCIe	128	4	0.037 ± 0.000
A100	256	8	0.054 ± 0.004
L40S	64	64	0.055 ± 0.001
<i>Consumer / Workstation</i>			
GeForce RTX 3090	64	64	0.066 ± 0.002
GeForce RTX 3060	64	2048	0.039 ± 0.000
GeForce RTX 3050 Ti	64	1024	0.031 ± 0.001
<i>Edge</i>			
Jetson Orin	256	256	0.088 ± 0.000

5.4. Results and Analysis

Kernel Parameter Optimization and Scalability Regimes. Performance is sensitive to the Bit-Sliced AES parameters: *Thread Size (TS)* and *Repeat Blocks (R)*. An exhaustive search was performed for each hardware configuration. Table 3 presents the kernel-only execution times for a standard "Large" astronomical image (≈ 600 MB).

A counter-intuitive observation from Table 3 is the parity between high-end datacenter GPUs (H100) and consumer hardware (RTX 3060) for the 600 MB dataset. This phenomenon indicates that for single-image processing of this size, the workload operates in a latency-bound regime. The massive parallelism of the H100 is underutilized, and the total time is dominated by constant system overheads (PCIe latency, kernel launch time, and I/O initialization) rather than raw arithmetic throughput.

To mitigate the impact of system overheads and evaluate the architectures in a throughput-bound regime, we extended the benchmark to an "Extra-Large" dataset (≈ 3.4 GB). This workload not only stresses the computational units but also tests the memory capacity limits of the devices. Table 4 details the End-to-End (E2E) performance for both file sizes.

The Cost of Integrity: GCM vs. CTR. Comparing the `Net GCM Cost` against `Net CTR Cost` allows us to isolate the computational overhead of the authentication layer. Across all architectures, GCM introduces a slowdown factor ranging from $\approx 3.0x$ to $4.5x$ compared to unauthenticated encryption. This reflects the unavoidable arithmetic cost of the finite field multiplications required for GHASH. Importantly, this ratio remains stable between the Large and Extra-Large datasets for high-end GPUs (e.g., H100 remains at $\approx 3.5x$), confirming that our parallel implementation scales linearly with data volume.

Comparison with CPU Baselines. While we focus on characterizing the GPU performance envelope, placing these results in context with CPU-based execution is essential. Recent state-of-the-art benchmarks for fully parallelized AES-GCM on GPUs

Table 4: Performance scalability analysis comparing Large (≈ 600 MB) and Extra-Large (≈ 3.4 GB) FITS files. The table decomposes the total End-to-End (E2E) time into a baseline I/O component (Astropy Time) and the Net GCM Cost (calculated as E2E Time - Astropy Time). This isolation reveals that while I/O masks performance differences on smaller files, the Net GCM Cost scales effectively on datacenter hardware for larger workloads. *Note: Consumer-grade and edge devices with limited VRAM (RTX 3060, 3050 Ti, and Jetson Orin) are excluded from the Extra-Large benchmark as the dataset size exceeds their available memory capacity.*

GPU Model	Astropy Time	E2E CTR Time	E2E GCM Time	Net CTR Cost	Net GCM Cost	GCM/CTR Net Ratio
<i>Large (≈ 600 MB)</i>						
H100 PCIe	0.104	0.462	1.304	0.358	1.200	3.35x
A100	0.256	0.477	1.240	0.221	0.984	4.46x
L40S	0.220	0.494	1.248	0.274	1.027	3.76x
GeForce RTX 3090	0.359	0.495	1.238	0.136	0.879	6.45x
GeForce RTX 3060	0.099	0.692	1.276	0.593	1.177	1.98x
GeForce RTX 3050 Ti	0.149	0.901	1.486	0.752	1.337	1.78x
Jetson Orin	0.226	0.662	1.765	0.435	1.539	3.53x
<i>Extra-Large (≈ 3.4 GB)</i>						
H100 PCIe	0.731	2.727	7.743	1.997	7.012	3.51x
A100	1.626	2.782	7.325	1.156	5.699	4.93x
L40S	1.098	3.007	7.678	1.910	6.580	3.45x
GeForce RTX 3090	0.978	2.875	7.099	1.897	6.121	3.23x

(Lee et al., 2025) demonstrate a speedup factor of $\approx 15\times$ compared to highly optimized multi-threaded CPU implementations (Intel Core i7 with AES-NI instructions using OpenSSL). Furthermore, the same study highlights a power efficiency advantage of over $20\times$ for the GPU architecture. Our results are consistent with this performance gap, validating the architectural choice of accelerator-based cryptography for massive datasets.

Throughput and Bottleneck Analysis. Figure 4 illustrates the time breakdown for the AES-GCM operation on the Large dataset. The results highlight a critical architectural insight: for files in the hundreds of megabytes range, the process is latency-bound. The GPU kernel execution time (blue) is a fraction of the total End-to-End time, which is dominated by system overheads and I/O (red).

This observation explains why a consumer-grade RTX 3060 can appear competitive with an H100 for single-image processing: for moderate file sizes, the workflow is dominated by system overheads rather than compute capacity.

However, as the dataset grows to the Extra-Large regime (Table 4), the performance hierarchy becomes clearer, though nuanced. The NVIDIA A100 asserts its advantage, achieving the lowest net processing cost (5.699 s), demonstrating excellent scalability. Interestingly, the RTX 3090 remains highly competitive (6.121 s), outperforming the H100 PCIe in this specific single-stream test, likely due to the RTX 3090’s massive memory bandwidth and the H100 PCIe’s bus constraints compared to its SXM counterparts. This behavior confirms that while specific hardware characteristics dictate the peak speed, GpuFitsCrypt effectively scales with the available hardware capability across both workstation and datacenter classes.

Scientific Validation via Photometry. To verify that the cryptographic process preserves the scientific utility of the data beyond mere bitwise integrity, we performed a photometric analysis using GPUPHOT, a high-performance photometry package currently under development (Alarcon and Lemes-Perera, in

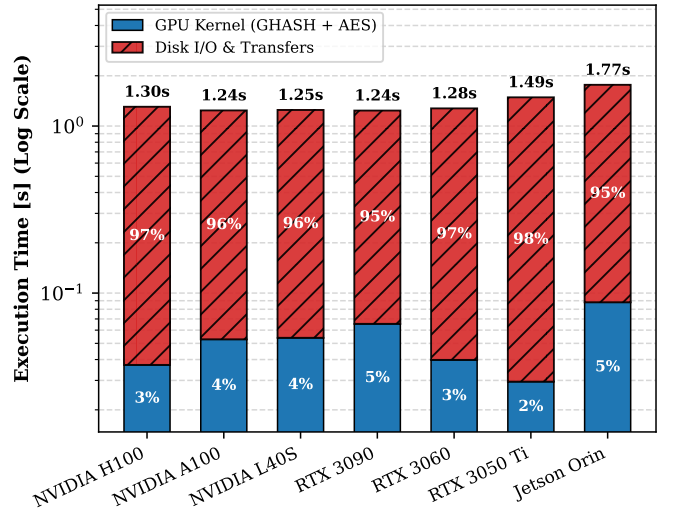


Figure 4: **Execution Time Breakdown for AES-GCM (Large File).** The chart illustrates the split between GPU Kernel Computation (Blue) and System/Disk I/O & Overhead (Red) on a logarithmic scale. For this moderate workload size (≈ 600 MB), the process operates in a latency-bound regime, where the GPU kernel accounts for a small fraction of the total execution time. This visualizes how system overheads and I/O latency dominate performance when the GPU is not fully saturated, explaining the parity between consumer and datacenter hardware in this specific scenario.

prep.). GPUPHOT integrates a novel set of convolution-based algorithms optimized for CUDA-enabled GPUs to accelerate point source photometry. We utilized a real scientific exposure from the Two-meter Twin Telescope (TTT3) containing a dense stellar field.

As illustrated in Figure 5, the validation confirms both security and utility. When applied to the encrypted payload (Panel b), the source extraction algorithm failed to converge, detecting zero sources due to the complete destruction of spatial structure. Conversely, the decrypted output (Panel c) yielded a source catalog identical to the original input. We compared critical parameters for all 182 detected sources, including centroid positions, Full Width at Half Maximum (FWHM ≈ 6.84 px), and instrumental flux, finding zero residuals. This confirms that the framework introduces no numerical artifacts, preserving the exact radiometric properties required for high-precision astronomy.

6. Discussion and Future Work

The results presented in this study demonstrate that the historical trade-off between rigorous security and high-performance data access in astronomy is no longer an insurmountable barrier. By leveraging the parallel processing capabilities of modern GPUs, we have shown that it is possible to implement authenticated encryption (AES-GCM) at speeds that match the I/O capabilities of standard storage infrastructure.

6.1. Latency vs. Throughput in Astronomical Pipelines

Our benchmarking reveals a distinct dichotomy between single-file latency and aggregate throughput. For interactive analysis of individual images (e.g., a researcher opening a 600 MB file), consumer-grade GPUs like the RTX 3090 or even the RTX 3060 provide performance indistinguishable from datacenter hardware, as the process is bound by I/O latency. This is a positive finding, as it lowers the barrier to entry for secure data access on standard workstations.

However, the value of Datacenter architectures (H100, A100) lies in their capacity for massive concurrency. While a single file does not saturate these cards, their massive VRAM and compute throughput allow for the processing of multiple streams simultaneously, a scenario typical of observatory pipelines reducing thousands of exposures per night. The scalability demonstrated in the Extra-Large benchmarks suggests that these architectures can handle petabyte-scale encryption without becoming a bottleneck.

6.2. Security Implications of the Architecture

Our framework's reliance on an external Key Management Service (KMS) is a deliberate architectural choice. It decouples the security policy from the data itself. Unlike password-protected ZIP files or static GPG keys, access to a dataset can be revoked instantly by updating the policy in the control plane, without needing to re-encrypt the petabytes of stored data. Furthermore, the use of GCM's integrity check prevents the "silent corruption" of scientific data, a risk in long-term archival storage that simple encryption methods do not address.

6.3. Limitations

The primary limitation of the current implementation is its dependency on the NVIDIA CUDA platform. While this covers a vast majority of HPC and workstation environments in astronomy, it excludes hardware from other vendors (AMD, Intel GPUs). Additionally, the requirement for pinned memory management, while essential for performance, requires careful integration into host applications to avoid memory exhaustion in highly concurrent multi-user environments.

6.4. Future Directions

Future work will focus on three key areas:

1. **Portability:** Porting the parallel GHASH reduction kernel to open standards like OpenCL or HIP/ROCm to support a wider range of hardware accelerators.
2. **Identity Federation:** Integrating the Access Control Module with federated identity providers (e.g., EduGain, ORCID) to facilitate seamless authentication for international collaborations.
3. **Attribute-Based Encryption:** Exploring advanced cryptographic schemes where policies are mathematically embedded into the ciphertext itself, potentially reducing the reliance on a centralized online Policy Engine for every transaction.

7. Conclusions

We have presented a high-performance framework for securing massive astronomical image catalogs. At its core is `GpuFitsCrypt`, a library that implements a novel parallel tree-reduction algorithm to accelerate AES-128-GCM on GPUs. This approach successfully overcomes the sequential bottleneck of the GHASH function, achieving end-to-end decryption throughputs that saturate standard storage interfaces.

Our architecture enables fine-grained, policy-based access control (e.g., role-based, temporal embargoes) while guaranteeing both the confidentiality and integrity of scientific data. By binding metadata context to the encrypted payload, we prevent tampering attacks that could compromise scientific validity. This work provides a path forward for data centers to enforce rigorous security during proprietary periods without hindering the pace of discovery, ultimately supporting a trusted and robust transition of data into the public domain.

CRediT authorship contribution statement

Samuel Lemes-Perera: Conceptualization, Methodology, Software, Validation, Formal analysis, Investigation, Data Curation, Writing - Original Draft, Visualization.

Miguel R. Alarcón: Methodology, Formal analysis, Visualization, Validation, Writing - Review & Editing.

Pino Caballero-Gil: Conceptualization, Supervision, Project administration, Writing - Review & Editing.

Miquel Serra-Ricart: Supervision, Resources, Validation, Writing - Review & Editing.

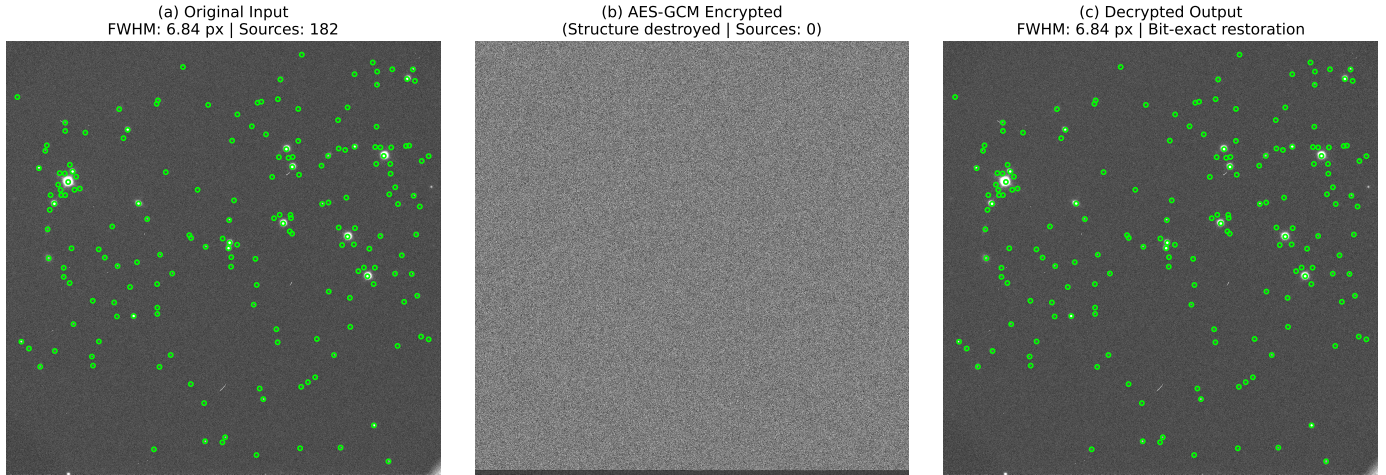


Figure 5: Visual validation of confidentiality and integrity using real scientific data. The test utilizes a raw exposure from the Two-meter Twin Telescope (TTT3). (a) The original FITS image allows the GPUHOT pipeline to detect 182 point sources with a mean FWHM of 6.84 pixels (green apertures). (b) The AES-GCM encrypted payload appears as high-entropy noise; the photometry software fails to identify any structure (0 sources detected), confirming semantic confidentiality. (c) The decrypted image is bitwise identical to the original, recovering the exact source catalog with identical photometric parameters.

Declaration of competing interest

The authors declare that they have no known competing financial interests or personal relationships that could have appeared to influence the work reported in this paper.

Software Availability

The source code for the GpuFitsCrypt library, including the GPU kernels and the Python wrapper, is available under an open-source license at <https://github.com/sllemesp/GpuFitsCrypt>. A persistent archive of the specific version used for the benchmarks presented in this paper will be deposited in Zenodo upon acceptance.

Acknowledgements

This work was supported by Light Bridges S.L. under an Industrial PhD agreement with the Universidad de La Laguna (ULL). S. Lemes-Perera acknowledges the funding and support provided by the company for this doctoral research.

The authors acknowledge support from the PID2022-138933OB-I00 ATQUE and 2023DIG28 IACTA research projects funded by MCIN/AEI/10.13039/501100011033/FEDER EU, and the CajaCanarias la Caixa Foundation, respectively. We also acknowledge the support provided by the CryptULL Research Group and the Cátedra de Ciberseguridad Binter-ULL for their contribution to the development of secure data management frameworks, as well as the institutional support provided by the Instituto Tecnológico y de Energías Renovables (ITER).

We express our gratitude to Light Bridges S.L. and ASTROPOC (<https://www.astropoc.com/>) for providing the high-performance GPU computing infrastructure, hardware resources, and astronomical datasets essential for the development, benchmarking, and performance evaluation of the GpuFitsCrypt library.

This article includes observations made in the Two-meter Twin Telescope (TTT) and Transient Survey Telescope (TST) both located at the Teide Observatory of the Instituto de Astrofísica de Canarias that Light Bridges operate on the island of Tenerife, Canary Islands (Spain). Dr. Antonio Maudes’s insights in economics and law were instrumental in shaping the development of this work.

Appendix A. Detailed Technical Resources

Appendix A.1. Code Listings

This appendix provides the essential Python implementations for both the scientific integration workflow and the performance benchmarking protocol used in this study.

Appendix A.1.1. Integration Workflow

Listing 1 illustrates how a scientist interacts with the library. It highlights the transparency of the solution: the complex GPU operations are abstracted, and the decrypted data is handed off to Astropy via zero-copy memory buffers.

Listing 1: Python integration workflow demonstrating granular access control. The code inspects the `warning_code` to handle partial decryption scenarios (e.g., embargoed data) without crashing, allowing metadata analysis even when the pixel payload is suppressed.

```

1 import ctypes
2 from astropy.io import fits
3
4 # 1. Interface with the high-performance C++/CUDA
5   backend
6 lib = ctypes.CDLL("./libgufitscrypt.so")
7
8 # 2. Initialize Context (Pre-allocate GPU resources)
9 context = lib.gfc_context_create(MAX_FILE_SIZE,
10                                MAX_FILE_SIZE)
11
12 try:
13     # 3. Decrypt and Authenticate (Parallel GPU
14       execution)

```

```

12 # Keys are typically retrieved from a KMS based on
13     user role
14 result = lib.gfc_decrypt_frame(context,
15     ENCRYPTED_FILE, key_h, key_d)
16
17 # 4. Granular Access Handling
18 if result.error_code == 0:
19     # Success: A valid FITS structure is available in
20     # memory
21     fits_bytes = ctypes.string_at(result.data_buffer,
22     result.buffer_size)
23
24     with fits.HDUList.fromstring(fits_bytes) as hdul:
25         # Check access level granted by the
26         # cryptographic engine
27         if result.warning_code == 0:
28             print("[FULL ACCESS] Processing
29             scientific pixel data...")
30             # ... perform photometry / source
31             # extraction ...
32
33         elif result.warning_code == 2:
34             # Scenario: User has Header Key but Data
35             # Key is invalid/embargoed
36             print("[PARTIAL ACCESS] Payload
37             Suppressed. Analyzing metadata only."
38             )
39             print("Target:", hdul[0].header['OBJECT'
40             ]) # Metadata is valid
41             # Pixel data is zero-filled; safe to read
42             # but contains no signal
43
44         elif result.warning_code == 1:
45             print("[FALLBACK] Header reconstruction.
46             Original metadata unavailable.")
47
48     else:
49         # Fatal Error: File corruption or system failure
50         print(f"[ERROR] Operation failed: {result.
51         error_message}")
52
53 finally:
54     lib.gfc_context_destroy(context)

```

Appendix A.1.2. Benchmarking Methodology

Listing 2 details the experimental protocol described in Section 5.3. Key features include the explicit separation of context initialization, the execution of discarded warm-up runs to stabilize the GPU state, and the isolation of the cryptographic overhead by subtracting the baseline I/O latency.

Listing 2: Benchmarking logic demonstrating the experimental protocol: baseline I/O measurement, context reuse, warm-up cycles, and steady-state timing.

```

1 import time
2 import numpy as np
3 from astropy.io import fits
4
5 # Configuration constants
6 NUM_WARMUP_RUNS = 5
7 NUM_TIMED_RUNS = 200
8
9 def measure_baseline_io(original_file):
10     """
11     Measures the baseline I/O performance (Astropy
12     Normal Open).
13     """
14     times = []
15     for _ in range(NUM_TIMED_RUNS):

```

```

15     start = time.monotonic()
16     # mmap=False forces actual disk I/O, ensuring a
17     # fair
18     # comparison against the decryption pipeline.
19     with fits.open(original_file, mode='readonly',
20     mmap=False) as hdul:
21         _ = hdul[0].data.shape # Force header parsing
22     times.append(time.monotonic() - start)
23     return np.median(times)
24
25 def run_benchmark_session(lib, encrypted_file, key_h,
26     key_d):
27     """
28     Executes the full benchmark protocol for a specific
29     configuration.
30     """
31     # 1. Context Initialization (Once per session)
32     # Allocates pinned memory and CUDA streams. Overhead
33     # excluded.
34     context = lib.gfc_context_create(MAX_SIZE, MAX_SIZE)
35
36     try:
37         # 2. Warm-up Phase (Discarded)
38         # Stabilizes GPU clocks and JIT compilation.
39         for _ in range(NUM_WARMUP_RUNS):
40             lib.gfc_decrypt_frame(context, encrypted_file
41             , key_h, key_d)
42
43         # 3. Steady-State Measurement Phase
44         latencies = []
45         for _ in range(NUM_TIMED_RUNS):
46             t_start = time.monotonic()
47
48             # Execute GPU Decryption & Authentication
49             result = lib.gfc_decrypt_frame(context,
50             encrypted_file, key_h, key_d)
51
52             t_end = time.monotonic()
53
54             if result.error_code == 0:
55                 latencies.append(t_end - t_start)
56
57         return np.median(latencies), np.std(latencies)
58
59     finally:
60         # 4. Resource Teardown
61         lib.gfc_context_destroy(context)
62
63     # Main Execution Flow
64     # -----
65     # A. Establish Baseline (I/O only)
66     baseline_io_time = measure_baseline_io("image_large.fits
67     ")
68
69     # B. Measure Cryptographic Performance (I/O + GPU +
70     # Overhead)
71     median_e2e, std_e2e = run_benchmark_session(lib, "
72     enc_image_large.fits", ...)
73
74     # C. Calculate Net Cost
75     net_crypto_cost = median_e2e - baseline_io_time
76     print(f"Net Cryptographic Cost: {net_crypto_cost:.4f} s"
77     )

```

Appendix A.2. Tables

Appendix A.3. Detailed Benchmark Configuration

To ensure reproducibility, we detail the hardware and software configuration used for all performance evaluations.

Table A.5: Detailed hardware specifications. Storage technology is a primary factor in I/O throughput bottlenecks during FITS processing.

Hostname	System Type	GPU Model (VRAM)	CPU Architecture	RAM	Storage Type
AAZ	HPC Node	NVIDIA H100 PCIe (80GB)	AMD EPYC 9124	62 GB	NVMe SSD
ALE	HPC Node	NVIDIA A100-SXM4 (80GB)	Intel Xeon Gold 6354	1 TB	NVMe SSD
AHP	HPC Node	NVIDIA L40S (48GB)	Intel Xeon Platinum 8468	251 GB	SAS SSD
TTT	Workstation	GeForce RTX 3090 (24GB)	Intel Core i9-10940X	125 GB	SATA HDD (RAID)
CCU	Desktop	GeForce RTX 3060 (12GB)	Intel Core i5-10400F	62 GB	NVMe SSD
LLB	Laptop	RTX 3050 Ti Mobile (4GB)	Intel Core i7-12700H	31 GB	NVMe SSD
JET	Edge Device	NVIDIA Jetson Orin AGX	ARMv8 (Cortex-A78AE)	8 GB	NVMe/eMMC

Table A.6: Synthetic FITS datasets for performance profiling. Sizes correspond to the pixel array payload (float32).

Category	Dimensions (px)	Pixels (10^6)	Size
Small	2048 × 2048	4.2	17 MB
Medium	7241 × 7241	52.4	201 MB
Large	14200 × 10650	151.2	577 MB
Extra Large	30000 × 30000	900.0	3.35 GB

Synthetic Dataset Generation. Benchmarks were conducted using a suite of real and synthetic FITS images. Synthetic images were generated via *Astropy* to mimic real scientific observations where specific sizes were needed. The pixel data consists of 32-bit floating-point numbers (BITPIX = -32) drawn from a Gaussian distribution ($\mu = 1500, \sigma = 200$). The headers include standard WCS telemetry, observation metadata and flux calibration. Table A.6 details the dimensions and sizes of the test files.

Hardware Environment. Benchmarks were executed on a diverse array of physical hosts, ranging from edge devices to HPC nodes. To ensure a consistent software environment, all tests were run within Docker containers based on `nvidia/cuda:12.0.1-devel-ubuntu22.04 (x86_64)` and `nvcr.io/nvidia/14t-cuda:12.2.12-devel (ARM64/Jetson)`, ensuring isolation and reproducibility. The detailed specifications are provided in Table A.5 (see above).

References

- Ade, P.A.R., et al., 2014. Detection of B-Mode Polarization at Degree Angular Scales by BICEP2. *Physical Review Letters* 112, 241101. doi:10.1103/PhysRevLett.112.241101.
- Ade, P.A.R., et al., 2015. Joint Analysis of BICEP2/Keck Array and Planck Data. *Physical Review Letters* 114, 101301. doi:10.1103/PhysRevLett.114.101301.
- An, S., Seo, S.C., 2020. Highly Efficient Implementation of Block Ciphers on Graphic Processing Units for Massively Large Data. *Applied Sciences* 10, 3711. URL: <https://www.mdpi.com/2076-3417/10/11/3711>, doi:10.3390/app10113711.
- Bellm, E.C., Kulkarni, S.R., Graham, M.J., Dekany, R., Smith, R.M., Riddle, R., Masci, F.J., Helou, G., Prince, T.A., Adams, S.M., Barbarino, C., Barlow, T., Bauer, J., Beck, R., Belicki, J., Biswas, R., Blagorodnova, N., Bodewits, D., Bolin, B., Brinnet, V., Brooke, T., Bue, B., Bulla, M., Burruss, R., Cenko, S.B., Chang, C.K., Connolly, A., Coughlin, M., Cromer, J., Cunningham, V., De, K., Delacroix, A., Desai, V., Duev, D.A., Eadie, G., Farnham, T.L., Feeny, M., Feindt, U., Flynn, D., Franckowiak, A., Frederick, S., Fremling, C., Gal-Yam, A., Gezari, S., Giomi, M., Goldstein, D.A., Golkhou, V.Z., Goobar, A., Groom, S., Hacopians, E., Hale, D., Henning, J., Ho, A.Y.Q., Hover, D., Howell, J., Hung, T., Huppenkothen, D., Imel, D., Ip, W.H., Ivezić, Ž., Jackson, E., Jones, L., Juric, M., Kasliwal, M.M., Kaspi, S., Kaye, S., Kelley, M.S.P., Kowalski, M., Kramer, E., Kupfer, T., Landry, W., Laher, R.R., Lee, C.D., Lin, H.W., Lin, Z.Y., Lunnan, R., Giomi, M., Mahabal, A., Mao, P., Miller, A.A., Monkevitz, S., Murphy, P., Ngeow, C.C., Nordin, J., Nugent, P., Ofek, E., Patterson, M.T., Penprase, B., Porter, M., Rauch, L., Rebbapragada, U., Reiley, D., Rigault, M., Rodriguez, H., Roestel, J.v., Rusholme, B., Santen, J.v., Schulze, S., Shupe, D.L., Singer, L.P., Soumagnac, M.T., Stein, R., Surace, J., Sollerman, J., Szkody, P., Taddia, F., Terek, S., Sistine, A.V., Velzen, S.v., Vestrand, W.T., Walters, R., Ward, C., Ye, Q.Z., Yu, P.C., Yan, L., Zolkower, J., 2019. The Zwicky Transient Facility: System Overview, Performance, and First Results. *Publications of the Astronomical Society of the Pacific* 131, 018002. URL: <http://arxiv.org/abs/1902.01932>, doi:10.1088/1538-3873/aaecbe. arXiv:1902.01932 [astro-ph].
- Berriman, G.B., Groom, S.L., 2011. How Will Astronomy Archives Survive the Data Tsunami? *Communications of the ACM* 54, 52–56. doi:10.1145/2043174.2043190.
- Brown, M.E., Barkume, K.M., Ragozzine, D., Schaller, E.L., 2007. A Collisional Family of Icy Objects in the Kuiper Belt. *Nature* 446, 294–296. doi:10.1038/nature05619.
- Brown, M.E., Trujillo, C.A., Rabinowitz, D.L., 2005. Discovery of a Planetary-Sized Object in the Scattered Kuiper Belt. *Astrophysical Journal Letters* 635, L97–L100. doi:10.1086/499336.
- Calabretta, M.R., Greisen, E.W., 2002. Representations of celestial coordinates in FITS. *Astronomy and Astrophysics* 395, 1077–1122. URL: <https://ui.adsabs.harvard.edu/abs/2002A&A...395.1077C>, doi:10.1051/0004-6361:20021327. aDS Bibcode: 2002A&A...395.1077C.
- Chambers, K.C., Magnier, E.A., Metcalfe, N., Flewelling, H.A., Huber, M.E., Waters, C.Z., Denneau, L., Draper, P.W., Farrow, D., Finkbeiner, D.P., Holmberg, C., Koppenhoefer, J., Price, P.A., Rest, A., Saglia, R.P., Schlafly, E.F., Smartt, S.J., Sweeney, W., Wainscoat, R.J., Burgett, W.S., Chastel, S., Grav, T., Heasley, J.N., Hodapp, K.W., Jedicke, R., Kaiser, N., Kudritzki, R.P., Luppino, G.A., Lupton, R.H., Monet, D.G., Morgan, J.S., Onaka, P.M., Shiao, B., Stubbs, C.W., Tonry, J.L., White, R., Bañados, E., Bell, E.F., Bender, R., Bernard, E.J., Boegner, M., Boffi, F., Botticella, M.T., Calamida, A., Casertano, S., Chen, W.P., Chen, X., Cole, S., Deacon, N., Frenk, C., Fitzsimmons, A., Gezari, S., Gibbs, V., Goessl, C., Goggia, T., Gourgue, R., Goldman, B., Grant, P., Grebel, E.K., Hambly, N.C., Hasinger, G., Heavens, A.F., Heckman, T.M., Henderson, R., Henning, T., Holman, M., Hopp, U., Ip, W.H., Isani, S., Jackson, M., Keyes, C.D., Koekemoer, A.M., Kotak, R., Le, D., Liska, D., Long, K.S., Lucey, J.R., Liu, M., Martin, N.F., Masci, G., McLean, B., Mindel, E., Misra, P., Morganson, E., Murphy, D.N.A., Obaika, A., Narayan, G., Nieto-Santesteban, M.A., Norberg, P., Peacock, J.A., Pier, E.A., Postman, M., Primak, N., Rae, C., Rai, A., Riess, A., Riffeser, A., Rix, H.W., Röser, S., Russel, R., Rutz, L., Schilbach, E., Schultz, A.S.B., Scolnic, D., Strolger, L., Szalay, A., Seitz, S., Small, E., Smith, K.W., Soderblom, D.R., Taylor, P., Thomson, R., Taylor, A.N., Thakar, A.R., Thiel, J., Thilker, D., Unger, D., Urata, Y., Valenti, J., Wagner, J., Walder, T., Walter, F., Watters, S.P., Werner, S., Wood-Vasey, W.M., Wyse, R., 2016. The Pan-STARRS1 Surveys. URL: <https://ui.adsabs.harvard.edu/abs/2016arXiv161205560C>, doi:10.48550/arXiv.1612.05560.
- Chen, T.X., Schmitz, M., Mazzarella, J.M., Wu, X., Van Eyken, J.C., Accomazzi, A., Akeson, R.L., Allen, M., Beaton, R., Berriman, G.B.,

- Boyle, A.W., Brouty, M., Chan, B.H.P., Christiansen, J.L., Ciardi, D.R., Cook, D., D'Abrusco, R., Ebert, R., Frayer, C., Fulton, B.J., Gelino, C., Helou, G., Henderson, C.B., Howell, J., Kim, J., Landais, G., Lo, T., Loup, C., Madore, B., Monari, G., Muench, A., Oberto, A., Ocvirk, P., Peek, J.E.G., Perret, E., Pevunova, O., Ramirez, S.V., Rebull, L., Shemmer, O., Smale, A., Tam, R., Terek, S., Van Orsow, D., Vannier, P., Wang, S.Y., 2022. Best Practices for Data Publication in the Astronomical Literature. *The Astrophysical Journal Supplement Series* 260, 5. URL: <https://iopscience.iop.org/article/10.3847/1538-4365/ac6268>, doi:10.3847/1538-4365/ac6268.
- Collaboration, T.A., 2013. *astropy v0.1: a core python package for astronomy*. URL: <https://zenodo.org/record/1461537>, doi:10.5281/ZENODO.1461537.
- Collaboration, T.A., 2018. *astropy v3.1: a core python package for astronomy*. URL: <https://zenodo.org/record/4080996>, doi:10.5281/ZENODO.4080996.
- Dworkin, M.J., 2007. Recommendation for block cipher modes of operation : GaloisCounter Mode (GCM) and GMAC. Technical Report NIST SP 800-38d. National Institute of Standards and Technology. Gaithersburg, MD. URL: <https://nvlpubs.nist.gov/nistpubs/Legacy/SP/nistspecialpublication800-38d.pdf>, doi:10.6028/NIST.SP.800-38d.edition:0.
- Green, R., Altieri, B., Blanton, M., Burns, E., Finke, J., Gao, P., Juric, M., Ostrenga, D., Rizzi, L., Shen, Y., Levy, R., 2024. Report of the Astrophysics Archives Review for the Astrophysics Division, Science Mission Directorate 12-14 March 2024. URL: <https://science.nasa.gov/wp-content/uploads/2024/10/nasa-aar2024-final-tagged.pdf>. place: Washington, DC.
- Greisen, E.W., Calabretta, M.R., 2002. Representations of world coordinates in FITS. *Astronomy and Astrophysics* 395, 1061–1075. URL: <https://ui.adsabs.harvard.edu/abs/2002A&A...395.1061G>, doi:10.1051/0004-6361:20021326. aDS Bibcode: 2002A&A...395.1061G.
- Greisen, E.W., Wells, D.C., Harten, R.H., 1980. The FITS Tape Formats: Flexible Image Transport Systems, Los Angeles. pp. 298–300. URL: <http://proceedings.spiedigitallibrary.org/proceeding.aspx?articleid=1230925>, doi:10.1117/12.959819.
- IAU FITS Working Group, 2016. Definition of the Flexible Image Transport System (FITS): The FITS Standard, Version 4.0. URL: https://fits.gsfc.nasa.gov/standard40/fits_standard40aa-1e.pdf. published: Standard document, International Astronomical Union.
- Ivezić, Ž., Kahn, S.M., Tyson, J.A., et al., 2019. LSST: From Science Drivers to Reference Design and Anticipated Data Products. *Astrophysical Journal* 873, 111. doi:10.3847/1538-4357/ab042c.
- Laureijs, R., Amiaux, J., Arduini, S., Auguères, J.L., Brinchmann, J., Cole, R., Cropper, M., Dabin, C., Duvet, L., Ealet, A., Garilli, B., Gondoin, P., Guzzo, L., Hoar, J., Hoekstra, H., Holmes, R., Kitching, T., Maciaszek, T., Mellier, Y., Pasian, F., Percival, W., Rhodes, J., Criado, G.S., Sauvage, M., Scaramella, R., Valenziano, L., Warren, S., Bender, R., Castander, F., Cimatti, A., Fèvre, O.L., Kurki-Suonio, H., Levi, M., Lilje, P., Meylan, G., Nichol, R., Pedersen, K., Popa, V., Lopez, R.R., Rix, H.W., Rotgering, H., Zeilinger, W., Grupp, F., Hudelot, P., Massey, R., Meneghetti, M., Miller, L., Paltani, S., Paulin-Henriksson, S., Pires, S., Saxton, C., Schrabback, T., Seidel, G., Walsh, J., Aghanim, N., Amendola, L., Bartlett, J., Baccigalupi, C., Beaulieu, J.P., Benabed, K., Cuby, J.G., Elbaz, D., Fos-alba, P., Gavazzi, G., Helmi, A., Hook, I., Irwin, M., Kneib, J.P., Kunz, M., Mannucci, F., Moscardini, L., Tao, C., Teyssier, R., Weller, J., Zamorani, G., Osorio, M.R.Z., Boulade, O., Foumond, J.J., Giorgio, A.D., Guttridge, P., James, A., Kemp, M., Martignac, J., Spencer, A., Walton, D., Blümchen, T., Bonoli, C., Bortoletto, F., Cerna, C., Corcione, L., Fabron, C., Jahnke, K., Ligori, S., Madrid, F., Martin, L., Morgante, G., Pampalona, T., Prieto, E., Riva, M., Toledo, R., Trifoglio, M., Zerbi, F., Abdalla, F., Douspis, M., Grenet, C., Borgani, S., Bouwens, R., Courbin, F., Delouis, J.M., Dubath, P., Fontana, A., Frailis, M., Grazian, A., Koppenhöfer, J., Mansutti, O., Melchior, M., Mignoli, M., Mohr, J., Neissner, C., Noddle, K., Poncet, M., Scodeggio, M., Serrano, S., Shane, N., Starck, J.L., Surace, C., Taylor, A., Verdoes-Kleijn, G., Vuerli, C., Williams, O.R., Zacchei, A., Altieri, B., Sanz, I.E., Kohley, R., Oosterbroek, T., Astier, P., Bacon, D., Bardelli, S., Baugh, C., Bellagamba, F., Benoist, C., Bianchi, D., Biviano, A., Branchini, E., Carbone, C., Cardone, V., Clements, D., Colombi, S., Conselice, C., Cresci, G., Deacon, N., Dunlop, J., Fedeli, C., Fontanot, F., Franzetti, P., Giocoli, C., Garcia-Bellido, J., Gow, J., Heavens, A., Hewett, P., Heymans, C., Holland, A., Huang, Z., Ilbert, O., Joachimi, B., Jennins, E., Kerins, E., Kiessling, A., Kirk, D., Kotak, R., Krause, O., Lahav, O., Leeuwen, F.v., Lescouargues, J., Lombardi, M., Magliocchetti, M., Maguire, K., Majerotto, E., Maoli, R., Marulli, F., Maurogordato, S., McCracken, H., McLure, R., Melchiorri, A., Merson, A., Moresco, M., Nonino, M., Norberg, P., Peacock, J., Pello, R., Penny, M., Pettorino, V., Porto, C.D., Pozzetti, L., Quercellini, C., Radovich, M., Rassat, A., Roche, N., Ronayette, S., Rossetti, E., Sartoris, B., Schneider, P., Semboloni, E., Serjeant, S., Simpson, F., Skordis, C., Smadja, G., Smartt, S., Spano, P., Spiro, S., Sullivan, M., Tilquin, A., Trotta, R., Verde, L., Wang, Y., Williger, G., Zhao, G., Zoubian, J., Zucca, E., 2011. Euclid Definition Study Report. URL: <http://arxiv.org/abs/1110.3193>, doi:10.48550/arXiv.1110.3193. issue: arXiv:1110.3193 arXiv:1110.3193 [astro-ph].
- Lee, J., Kim, D., Seo, S.C., 2025. Parallel implementation of GCM on GPUs. *ICT Express* 11, 310–316. URL: <https://linkinghub.elsevier.com/retrieve/pii/S2405959525000062>, doi:10.1016/j.ict.2025.01.006.
- Lee, W.K., Seo, S.C., Seo, H., Kim, D.C., Hwang, S.O., 2024. Speed Record of AES-CTR and AES-ECB Bit-Sliced Implementation on GPUs. *IEEE Embedded Systems Letters* 16, 481–484. URL: <https://ieeexplore.ieee.org/document/10549968/>, doi:10.1109/LES.2024.3409725.
- Manavski, S.A., 2007. CUDA Compatible GPU as an Efficient Hardware Accelerator for AES Cryptography, in: *IEEE International Conference on Signal Processing and Communications (ICSPC)*, pp. 65–68. doi:10.1109/ICSPC.2007.4728256.
- McGrew, D.A., Viega, J., 2004. The Galois/Counter Mode of Operation (GCM). Submission. NIST Modes of Operation Process. URL: <https://csrc.nist.gov/groups/ST/toolkit/BKM/documents/proposedmodes/gcm/gcm-revised-spec.pdf>.
- National Radio Astronomy Observatory, 2022. ALMA Services Affected by Cyberattack. URL: <https://public.nrao.edu/news/alma-services-affected-by-cyberattack/>.
- Ponz, J.D., Thompson, R.W., Munoz, J.R., 1994. The FITS image extension. *Astronomy and Astrophysics Supplement Series* 105, 53–55. URL: <https://ui.adsabs.harvard.edu/abs/1994A&AS...105...53P>. aDS Bibcode: 1994A&AS...105...53P.
- Salowe, J., Choudhury, A., McGrew, D., 2008. AES Galois Counter Mode (GCM) Cipher Suites for TLS. Technical Report RFC5288. RFC Editor. URL: <https://www.rfc-editor.org/info/rfc5288>, doi:10.17487/rfc5288.
- Wells, D.C., Greisen, E.W., Harten, R.H., 1981. FITS - a Flexible Image Transport System. *Astronomy and Astrophysics Supplement Series* 44, 363. URL: <https://ui.adsabs.harvard.edu/abs/1981A&AS...44...363W>. aDS Bibcode: 1981A&AS...44...363W.
- Wilkinson, M.D., Dumontier, M., Aalbersberg, I.J., Appleton, G., Axton, M., Baak, A., Blomberg, N., Boiten, J.W., Da Silva Santos, L.B., Bourne, P.E., Bouwman, J., Brookes, A.J., Clark, T., Crosas, M., Dillo, I., Dumon, O., Edmunds, S., Evelo, C.T., Finkers, R., Gonzalez-Beltran, A., Gray, A.J., Groth, P., Goble, C., Grethe, J.S., Heringa, J., 'T Hoen, P.A., Hooft, R., Kuhn, T., Kok, R., Kok, J., Lusher, S.J., Martone, M.E., Mons, A., Packer, A.L., Persson, B., Rocca-Serra, P., Roos, M., Van Schaik, R., Sansone, S.A., Schultes, E., Sengstag, T., Slater, T., Strawn, G., Swertz, M.A., Thompson, M., Van Der Lei, J., Van Mulligen, E., Velterop, J., Waagmeester, A., Wittenburg, P., Wolstencroft, K., Zhao, J., Mons, B., 2016. The FAIR Guiding Principles for scientific data management and stewardship. *Scientific Data* 3. URL: <https://www.nature.com/articles/sdata201618>, doi:10.1038/sdata.2016.18.
- Yao, Y., Miller, A.A., Kulkarni, S.R., Bulla, M., Masci, F.J., Goldstein, D.A., Goobar, A., Nugent, P., Dugas, A., Blagorodnova, N., Neill, J.D., Rigault, M., Sollerman, J., Nordin, J., Bellm, E.C., Cenko, S.B., De, K., Dhawan, S., Feindt, U., Fremling, C., Gatkine, P., Graham, M.J., Graham, M.L., Ho, A.Y.Q., Hung, T., Kasliwal, M.M., Kupfer, T., Laher, R.R., Perley, D.A., Rusholme, B., Shupe, D.L., Soumagnac, M.T., Taggart, K., Walters, R., Yan, L., 2019. ZTF Early Observations of Type Ia Supernovae. I. Properties of the 2018 Sample. *The Astrophysical Journal* 886, 152. URL: <https://ui.adsabs.harvard.edu/abs/2019ApJ...886..152Y>, doi:10.3847/1538-4357/ab4cf5. aDS Bibcode: 2019ApJ...886..152Y.